CrossMark

Temporal expectations and neural amplitude fluctuations in auditory cortex interactively influence perception

Björn Herrmann [a,*], Molly J. Henry [a], Saskia Haegens [b,c], Jonas Obleser [a,d]

[a] Max Planck Research Group "Auditory Cognition", Max Planck Institute for Human Cognitive and Brain Sciences, Stephanstraße 1A, 04103 Leipzig, Germany
[b] Department of Psychiatry, Columbia University College of Physicians and Surgeons, New York, NY 10032, USA
[c] Cognitive Neuroscience and Schizophrenia Program, Nathan S. Kline Institute, 140 Old Orangeburg Road, Orangeburg, NY 10962, USA
[d] Department of Psychology, University of Lübeck, Ratzeburger Allee 160, 23562 Lübeck, Germany

ARTICLE INFO

ABSTRACT

Alignment of neural oscillations with *temporally regular* input allows listeners to generate temporal expectations. However, it remains unclear how behavior is governed in the context of *temporal variability*: What role do temporal expectations play, and how do they interact with the strength of neural oscillatory activity? Here, human participants detected near-threshold targets in temporally variable acoustic sequences. Temporal expectation strength was estimated using an oscillator model and pre-target neural amplitudes in auditory cortex were extracted from magnetoencephalography signals. Temporal expectations modulated target-detection performance, however, only when neural delta-band amplitudes were large. Thus, slow neural oscillations act to gate influences of temporal expectation on perception. Furthermore, slow amplitude fluctuations governed linear and quadratic influences of auditory alpha-band activity on performance. By fusing a model of temporal expectation with neural oscillatory dynamics, the current findings show that human perception in temporally variable contexts relies on complex interactions between multiple neural frequency bands.

© 2015 Elsevier Inc. All rights reserved.

Introduction

Low-frequency neural oscillations are periodic voltage or field variations of neural populations, and reflect fluctuations in neural excitability (Bishop, 1933; Kayser et al., 2015; Lakatos et al., 2005). Consistent with these cyclic excitability fluctuations, the probability of detecting near-threshold sensory events has been shown to depend on the neural phase into which an event falls (Busch et al., 2009; Busch and VanRullen, 2010; Hanslmayr et al., 2013; Henry and Obleser, 2012; Monto et al., 2008; Ng et al., 2012). For sensory input characterized by temporal regularity, low-frequency neural oscillations synchronize with the pattern of event onsets occurring over time through adjustments of the oscillation's phase and period (i.e., neural entrainment). Neural entrainment brings high-excitable phases into alignment with attended or high-energy portions of the input (Lakatos et al., 2008, 2013; Thut et al., 2011), and is thereby proposed to organize the phase–behavior relation (Henry et al., 2014; Neuling et al., 2012).

Variations in the strength of low-frequency neural oscillations (i.e., amplitude envelope fluctuations) relate to the overall strength of neural excitability fluctuations: High amplitudes correspond to more

drastic fluctuations in excitability than low amplitudes (Fig. 1, Jensen and Mazaheri, 2010). Furthermore, for measurements made at the scalp, neural amplitude is also a reflection of the number of neurons whose excitability fluctuations are temporally synchronized (Musall et al., 2014). In turn, the degree of synchrony among neuronal populations relates to the degree of neural entrainment and thus depends on the degree of temporal regularity in the environmental stimulus (Schroeder and Lakatos, 2009b; Thut et al., 2011).

Temporal regularity in the sensory input gives rise to temporal expectations, meaning that the time of occurrence of an upcoming sensory event can be expected. Conceptually, a sequence's temporal regularity is linked to temporal expectations via oscillatory dynamics (Arnal and Giraud, 2012; Henry and Herrmann, 2014; Schroeder and Lakatos, 2009b). That is, a listener needs an internal model on the basis of which external events can be judged as temporally (un)expected (Jones and Boltz, 1989; McAuley and Jones, 2003). This internal model can be conceptualized as a simple oscillator capable of synchronizing with a stimulus sequence (Canavier, 2015; Large and Jones, 1999). Specifically, the phase of an oscillation synchronized with the external event structure quantifies the timing of an expected event, that is, a temporal expectation (Henry and Herrmann, 2014). In turn, when a stimulus event fails to coincide with the expected event onset, the temporal expectation is violated. Phase can be estimated from measured neural oscillatory activity (Henry et al., 2014; Schroeder and Lakatos, 2009b), which

* Corresponding author at: Brain and Mind Institute, University of Western Ontario, London, Ontario N6A 5B7, Canada.
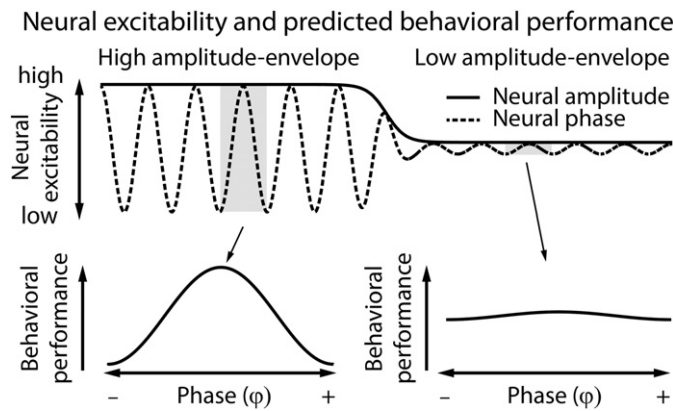*E-mail address:* herrmann.b@gmail.com (B. Herrmann).

Fig. 1. Neural excitability and predicted behavior. Schematic display of neural excitability fluctuations, the corresponding amplitude envelope changes, and predicted perceptual performance for high and low neural amplitudes as a function of phase/temporal expectation (which was estimated from the oscillator model exemplified in Fig. 2).

emphasizes the relation to neural excitability. However, phase can also be estimated from the external event structure using a mathematical oscillator model (Large and Jones, 1999; McAuley and Jones, 2003), which emphasizes the relation to temporal expectations, and avoids the possibility of poor neural phase estimation for low neural amplitude values (Muthukumaraswamy and Singh, 2011). That is, modeled phase and neural amplitude are estimated independently.

Previous studies investigating the effects of temporal expectations on neural and behavioral responses have reported enhanced perceptual performance in temporally regular compared to irregular stimulation sequences (Cravo et al., 2013; Lange, 2009; Lawrance et al., 2014; Rohenkohl et al., 2012). However, single events in temporally irregular sequences can still be temporally expected to varying degrees based on the local temporal structure (Jones and Yee, 1997). Furthermore, temporal expectations might also be important for perception of natural stimuli such as speech or music (Giraud and Poeppel, 2012; Peelle and Davis, 2013). However, speech and music are not strictly periodic and thus continuously modulate (1) the degree to which low-frequency oscillations are entrained, (2) the strength with which neural excitability fluctuates, and (3) the extent to which temporal expectations can be generated.

In the current magnetoencephalography (MEG) study, we used temporally variable tone sequences to investigate four thus far unanswered questions: (1) Is perceptual performance affected by temporal expectations in stimulus sequences with temporal variation? (2) Do performance effects stemming from variations in the strength of temporal expectations depend on low-frequency neural amplitude (i.e., strength of excitability fluctuations and/or synchrony of neural populations)? (3) Previous studies also reported that amplitude fluctuations, for example, in alpha and beta frequency bands affect perception in temporal context (Arnal et al., 2015; Fujioka et al., 2012; Rohenkohl and Nobre, 2011; Saleh et al., 2010). Thus, we asked: Does perceptual performance in temporally variable tone sequences also depend on neural amplitude variations in non-entrained frequency bands? (4) Finally, recent work has shown complex effects of cross-frequency relations on perceptual performance for phase–phase interactions (Fiebelkorn et al., 2013; Henry et al., 2014) and phase–amplitude coupling (Arnal et al., 2015; Friese et al., 2013). Here we focused on neural amplitude, and asked: Do neural amplitude fluctuations in multiple frequency bands jointly influence performance?

The data revealed a joint influence of temporal expectations and low-frequency neural amplitude variations as well as interactive influences of neural amplitudes in multiple frequency bands on perceptual performance.

Methods and materials

Participants

Twenty adult humans participated in the current MEG study (mean age: 26.2 years, SD: 2.9 years; 10 females). Participants were native speakers of German and were financially compensated for their participation (7 Euros per hour). They did not report any neurological diseases or any hearing problems, and gave written informed consent prior to the experiment. The study was in accordance with the Declaration of Helsinki and approved by the local ethics committee of the University of Leipzig.

Acoustic stimulation and procedure

During the MEG recording, participants were presented with tone sequences containing intensity deviants (target tones; Fig. 2). Non-target tones in the experiment were presented at 50 dB above the individual hearing threshold (i.e., sensation level), which was determined prior to the MEG experiment using the method of limits. Sound intensity of target tones was slightly louder and titrated individually for each participant prior to the experiment to yield on average 65% detection rate (mean target–to–non-target intensity difference: $+2.44$ dB $\pm$ 0.29 SD; titration was done using similar tone sequences as for the MEG experiment). Note that in the current design, 65% detection rate is far above chance level due to the continuous nature of the sequence.

Tone sequences consisted of 25 1000-Hz sine tones, each 100 ms in duration (5 ms linear rise and fall times). Each sequence contained 2, 3, or 4 target tones at random locations within a sequence and participants were instructed to press a button when they heard a tone that was louder than the others. Responses were considered hits when they occurred within 0.2–1.2 s after target onset. Randomization of target occurrence was constrained such that the first three and the last two tones could never be a target. Furthermore, there were at least three non-target tones between two consecutive targets.

Stimulation frequency was on average 2 Hz ($\pm$ 0.14 Hz SD), while the exact onset-to-onset intervals were randomly jittered. That is, within each sequence, tones occurred on average every 500 ms, but
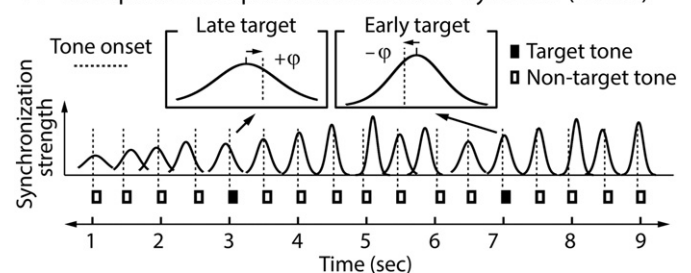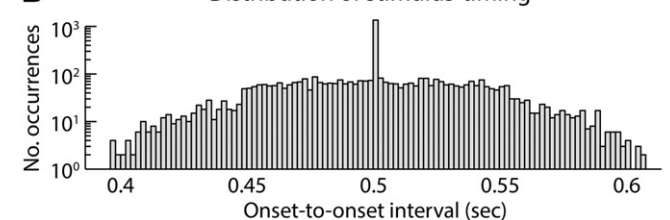

Fig. 2. Experimental stimulation. (A) An example segment of a tone sequence and modeled oscillator dynamics (Large and Jones, 1999). The distance between the peak of the modeled oscillation and the target onset indicates the degree to which a target is temporally expected and is referred to as relative phase (φ). Synchronization strength reflects the degree to which the oscillator is entrained by the stimulation. (B) Distribution of onset-to-onset intervals presented to one participant.

individual tone onsets were jittered within a range of ±55 ms. As a result, onset-to-onset intervals ranged from minimally 390 ms (when a late tone was followed by an early tone) to maximally 610 ms (when an early tone was followed by a late tone; Fig. 2B). Temporally jittered stimulus presentation still entrains neural oscillations in auditory cortex but leads to more variable neural phase distributions compared to iso-chronous stimulation (Besle et al., 2011). Critically, the onset-to-onset interval directly before and directly after each target tone was fixed at 500 ms in order to avoid perceptual foreperiod or masking (forward and backward) effects (see Cravo et al., 2013). Furthermore, target positions were fixed at multiples of the average stimulation interval (0.5 s). Hence, whether or not a target is detected cannot be related to tracking multiples of the stimulation interval (or an average tracking strategy).

Individual sequences, lasting approximately 12.5 s each, were separated by a silent inter-trial interval lasting 2.667 s. In six blocks, participants listened to a total of 216 sequences (36 per block) and were presented with 648 target tones. The experiment lasted approximately 150 min including preparation of the MEG recordings.

Behavioral data: model-based estimation of temporal expectation

In the current study, each tone sequence exhibited some temporal variability. The temporal context leading up to a target tone thus varied, although the onset-to-onset interval directly prior to and directly after a target was held constant at precisely 0.5 s and targets occurred at multiples of the average stimulation interval (0.5 s; 2 Hz). We hypothesized that an intensity deviant would be more likely to be detected when it occurred at a time that was predictable given the preceding temporal context, relative to when it occurred at an unexpected time.

We formalized this prediction based on the mathematical oscillator model described by Large and Jones (1999), which was used to estimate the relative phase (φ) of an oscillation with respect to each tone in each individual sequence heard by a participant, independent of MEG data (Fig. 2A). The modeled oscillator phase (φ, bound between −0.5 and 0.5) provides a measure of the difference between the expected onset time of a tone and the actual tone onset, that is, the degree to which a tone onset is (un)expected. Specifically, modeled phase values close to zero indicate good correspondence between the actual (physical) tone onset and its expected onset, while larger-magnitude values indicate that the tone onset would have been relatively unexpected (negative relative phase indicates that the target was early; positive relative phase indicates that the target was late; Fig. 2A). For details on the mathematical implementation of the oscillator model see Large and Jones (1999).

Modeled phase values for tone onsets within each sequence were calculated as follows. Model parameters were chosen so that the oscillator most strongly adjusted its phase in response to tone onsets, and adjusted its period to a lesser degree (coupling strength 1 and 0.3, respectively; Inden et al., 2012; Large and Jones, 1999; synchronization strength could be ignored for the current analyses). For each sequence, the oscillator's initial period was set to 0.5 s (2 Hz; the average stimulation rate), and the oscillator's initial phase (relative to the first tone onset in a sequence) was chosen randomly to take on one value within a half cycle centered on zero phase lag. All random initial phase values allowed quick entrainment of the oscillator by tones within a sequence, in line with recent simulations and recordings of neural oscillations (Ali et al., 2013; Fröhlich and McCormick, 2010). Subsequently, the modeled phase values (φ) for single-trial target tones were divided into 15 overlapping percentile bins (width: 30%; for a similar approach see Cravo et al., 2013) and the proportion of correct responses (hit rate) was calculated for each bin (Fig. 3).

In order to account for the random selection of the oscillator's initial phase values (relative to the first tone in a sequence), estimation of modeled phase values (φ) for each tone in each sequence, dividing phase values for target tones into 15 bins, and calculation of hit rates
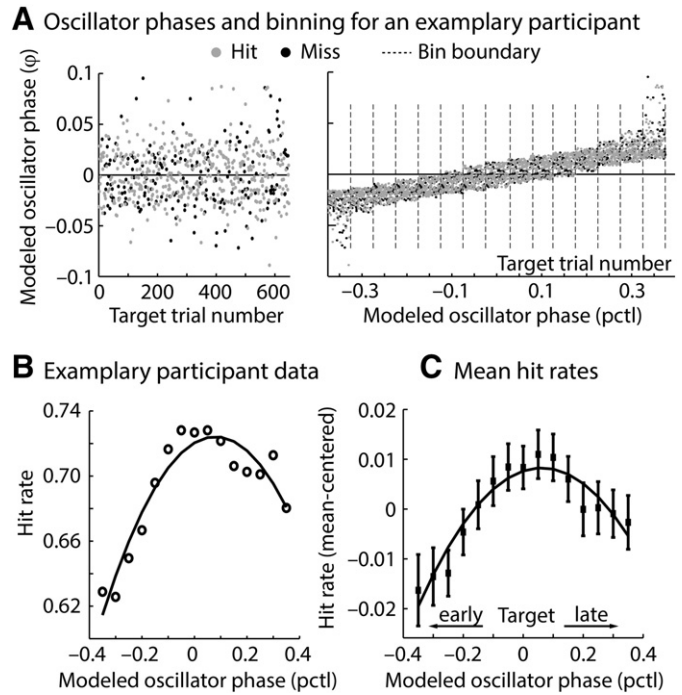

Fig. 3. Behavioral results. (A) Binning of single-trial modeled oscillator phase values for one example participant. Left: modeled phase for each target trial. Right: phase values sorted into 15 phase percentile bins (pctl). Note that here the overall number of trials is larger than in the left panel due to overlap of the bins. (B) Hit rate as a function of oscillator phase percentile bin and the corresponding quadratic fit for the same participant depicted in (A). (C) Mean hit rates (across participants; mean-centered) for each oscillator phase percentile bin. Error bars reflect the standard error of the mean (SEM).

was repeated 500 times. In a final step, hit rates for each of the 15 bins were averaged across repetitions.

Behavioral data: statistical analysis

Although the modeled oscillator phase is a circular variable, we here treat phase values linearly for two reasons: (1) modeled phase values reflect the *relative* phase between the peak of the oscillation and the physical tone onset, and thus reflect a distance measure with a meaningful center (i.e., target onset and peak of the oscillation coincided); and (2) modeled phase values (before binning) were well within the limits of one cycle (i.e., greater than −0.5 and smaller than 0.5) due to the specific jitter used in the current study (±55 ms). Thus, for the statistical analysis, a quadratic trend analysis was carried out in order to test whether hit rate was highest when the physical target onset co-incided with the peak phase of the oscillation (expected onset), relative to when the target occurred too early (negative phase) or too late (positive phase). That is, for each participant, a quadratic function was fitted to hit rates as a function of binned modeled oscillator phase (i.e., temporal expectations; Fig. 3B) using a least-squares routine. To test for a quadratic modulation of target-detection performance, the estimated quadratic coefficients were subsequently tested against zero using a one-sample *t*-test. Throughout the manuscript, effect sizes are reported as $r_{equivalent}$ (Rosenthal and Rubin, 2003; hereafter referred to as simply *r*), which is equivalent to a Pearson product–moment correlation for two continuous variables, to a point–biserial correlation for one continuous and one dichotomous variable, and to the square root of partial η^2 (eta-squared) for ANOVAs.

MEG recording and preprocessing

Participants' magnetoencephalograms were recorded in an electro-magnetically shielded room (Vacuumschmelze, Hanau, Germany)

using a 306-channel Neuromag Vectorview MEG (Elekta, Helsinki, Finland) at a sampling rate of 1000 Hz, with a passband ranging from DC to 330 Hz. The position of the participant's head was continuously measured by five head position indicator coils (mean movement per block: 3 mm). The signal space separation method was applied offline in order to suppress external interferences, interpolate bad channels, and transform individual data to a common sensor space that allows comparisons across participants (Taulu et al., 2004). Data analysis was carried out using custom MATLAB (v7.11; MathWorks, Inc.) scripts. In the current study, only the 204 orthogonal planar gradiometers in 102 locations were used, as they are most sensitive to magnetic fields originating from sources directly below them (Hämäläinen et al., 1993).

In order to identify artifacts such as eye movements, heart activity and noisy channels, preprocessing was first geared towards computing independent components analysis (ICA) using Fieldtrip software (http://fieldtrip.fcdonders.nl/; v20130727; Oostenveld et al., 2011). Preprocessing included high-pass filtering (0.7 Hz, 2391 points, Hann window) and low-pass filtering (100 Hz, 151 points, Kaiser window), down-sampling to 250 Hz, dividing recordings into epochs (−4 to 4 s around target onset), and submitting the data to ICA (principle component dimension reduction; runica method Makeig et al., 1996; logistic infomax algorithm Bell and Sejnowski, 1995). Components reflecting artifacts were identified (by visual inspection) as well as components showing clear occipital/posterior activity and a peak in the amplitude spectrum in the alpha frequency range (8–13 Hz). Identification and subsequent removal (see below) of alpha components were done in order to avoid rejecting a large number of trials in the signal-range artifact rejection procedure following ICA and to optimize the current analysis approach towards oscillatory activity in auditory cortex. The "unmixing" matrix and the "mixing" matrix from ICA as well as the to-be-removed component numbers were saved (median removed components [interquartile range]: 14 [6]).

High-pass filtered data are advantageous for identification of ICA components. However, for our analyses we wanted to avoid "smearing" of variations in target-related activity into the pre-target time window by using a high-pass filter. Thus, we went back to the original data, repeating the previous steps except that high-pass filtering was omitted. In detail, data were low-pass filtered (100 Hz, 151 points, Kaiser window; note that the low-pass filter is very short and thus post-target

onset activity does not affect pre-target activity), down-sampled to 250 Hz, divided into epochs (−4 to 4 s around target onset), and detrended using linear regression. Data were subsequently projected to ICA space (using the unmixing matrix), and after removal of the previously identified components projected back to the original 204 MEG channels (using the mixing matrix from the previously described pipeline). Finally, epochs were excluded if the signal range was larger than 300 pT/m in any of the gradiometer channels (median excluded trials [interquartile range]: 5 [6]). Only data from this preprocessing pipeline were used for further analyses.

MEG data analysis: spatial filtering and source localization

In order to reduce the high-dimensional MEG data and to focus our analysis on auditory cortex neural activity, a spatial filter was constructed for each participant (for comparable approaches see de Cheveigné and Simon, 2008; Garrido et al., 2013). In detail, for each MEG channel, time domain signals (−4 to 4 s epochs) were averaged across all trials, multiplied with a Hann window, and a fast Fourier transform (FFT) was calculated (see Fig. 4 for the corresponding amplitude spectrum). The resulting complex coefficients at 2-Hz (i.e., the average stimulation frequency) were used to calculate a cross-spectral density matrix. A singular value decomposition was then computed using the cross-spectral density matrix, and the real part of the first eigenvector's elements were used as spatial filter weights. Finally, single-trial time-domain data were projected onto the virtual source using the spatial filter.

Note that similar to other spatial filter approaches such as ICA (Makeig et al., 1996), beamformer (Gross et al., 2001), or signal-space projection (Tesche et al., 1995; Uusitalo and Ilmoniemi, 1997), the current spatial filter suppresses neural activity unrelated to the target source. The specific assumptions on which the construction of the filter is based differ between approaches, but here are constrained by the neural activity at the average stimulation frequency of 2 Hz.

In order to confirm that the sources underlying the spatial filter originate in auditory cortices, an anatomically constrained source localization was calculated for the spatial filter. Individual T1-weighted MR images (3 T Magnetom Trio, Siemens AG, Germany) were used to construct inner skull surfaces (volume conductor) and mid-gray matter cortical surfaces (source model; using Freesurfer and MNE software).
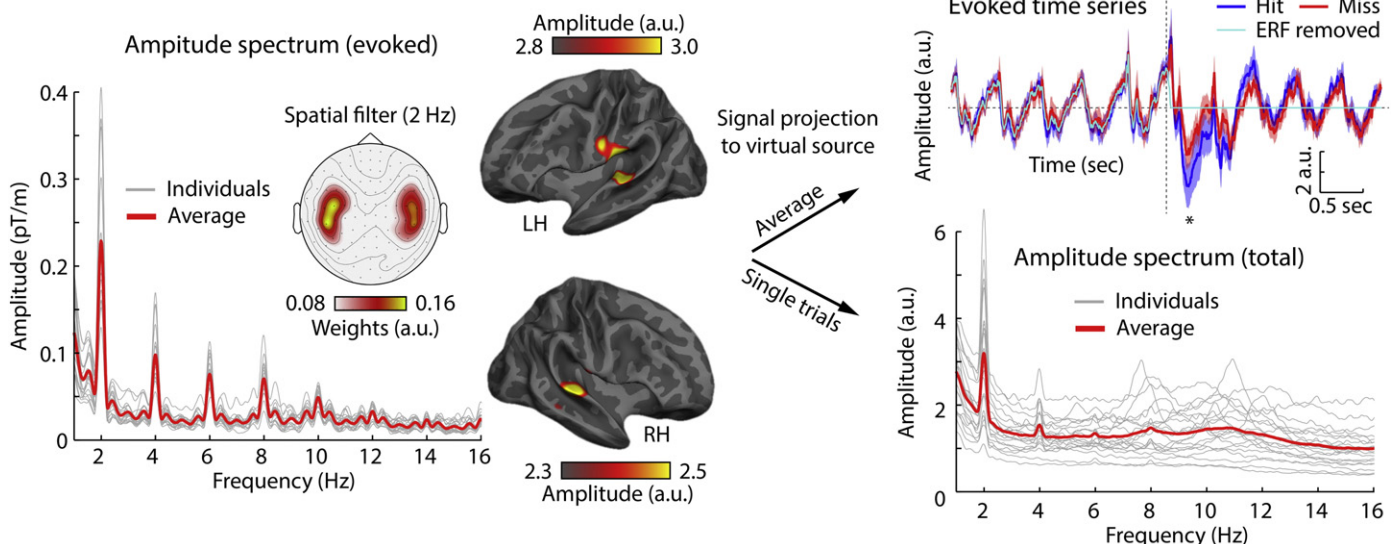

Fig. 4. Brain signals in sensor space, source space, and for the virtual source after spatial filtering. Left: mean evoked amplitude spectrum (averaged across channels) from a fast Fourier transform (FFT) calculated from trial-averaged time series. Spatial filter calculated from the 2-Hz complex coefficients of the spectrum. Middle: source localization of the spatial filter topography using sLORETA. Right: data projected through the spatial filter to the auditory cortex virtual channel. Top: trial-averaged (evoked; −2.5 to 2.5 s) time series for hits (blue) and misses (red). Shaded portions reflect the SEM. Target onset is marked by the crossing of the dashed lines. For visual purposes, a high-pass filter of 0.2 Hz was applied to the time series. The asterisk indicates a significant (P < 0.05) amplitude difference between hits and misses for the 0.16 to 0.36 s time interval. Bottom: amplitude spectrum (total) calculated from single-trial time series using a FFT, and subsequent averaging across trials. a.u. — arbitrary units.

The MR and the MEG coordinate systems were co-registered using the MNE software (http://www.martinos.org/mne/) which included an automated and iterative procedure that fitted the approximately 200 digitized head surface points (Polhemus FASTRAK 3D digitizer) to the MR reconstructed head surface (Besl and McKay, 1992). Lead fields were calculated from a boundary element model (inner skull; Nolte, 2003) using MNE software and Fieldtrip software, and inverse solutions were calculated using sLORETA (Pascual-Marqui, 2002) using custom MATLAB scripts. Differences in overall brain activation strength between participants were reduced by global mean normalization, which involved dividing the activation at each vertex by the mean activity across all vertices. Neural activity was spatially smoothed across the surface using an approximation to a 6 mm FWHM Gaussian kernel (Han et al., 2006). Individual cortical representations were transformed to a common coordinate system (Fischl et al., 1999b), and finally morphed to the partially inflated cortical surface of the Freesurfer standard brain (Fischl et al., 1999a).

MEG data analysis: pre-target oscillatory neural activity

All analyses of neural responses were conducted using the spatially filtered single-trial signals and focused on pre-target oscillatory amplitude fluctuations. Neural phase was not investigated in the current study. The arbitrariness of the sign of spatially filtered time domain signals (between participants) related to the singular value decomposition during filter construction could potentially harm an analysis of neural phase across participants.

In order to analyze pre-target neural oscillatory activity we first removed all target-related evoked responses from the single-trial time domain data. To this end, the time-domain signal following target onset was muted by multiplying it with half of a Hann window that ranged from 0 to 0.05 s, and was zero thereafter (for a similar approach see Henry et al., 2014; Lakatos et al., 2013). This was done in order to exclude temporal "smearing" of potential variations in evoked responses to target tones into the pre-target time interval by the wavelet convolution. A Hann window was chosen due to its wide application in spectral analyses and filter designs (Nitschke et al., 1998; Wallisch et al., 2009). As a consequence, any relation between pre-target neural activity and behavioral performance (see below) cannot be due to temporal smearing of post-target onset variations of neural activity (Henry et al., 2014; Lakatos et al., 2013; O'Connel et al., 2014). Furthermore, subsequent analyses of neural amplitude were based on percentiles and thus were insensitive to the overall magnitude of neural responses (see below), and were thus unaffected by any amplitude dampening introduced by this procedure.

Next, time–frequency representations were calculated using a wavelet approach, where single-trial time series (-4 to 4 s) were convolved with Morlet wavelets (Tallon-Baudry et al., 1996). Single-trial time–frequency representations were calculated for the -0.3 to 0 s pre-target time interval (in steps of 0.004 s) and the 1–20-Hz frequencies (in steps of 0.2 Hz) using a wavelet family with a constant ratio of $f/\sigma f = 6.28$ (Tallon-Baudry et al., 1996). Single-trial time–frequency neural amplitudes were calculated as the magnitude of the resulting complex wavelet transform coefficients, which in turn were used for subsequent analyses.

MEG data analysis: low-frequency neural oscillations and temporal expectations

In a first analysis, we focused on 2-Hz neural activity within a time window of a few samples directly prior to target onset. That is, independently for each time point within the 0.03 s prior to target onset, single trials were sorted into a 15 × 15 grid of overlapping percentile bins (width: 30%) according to the instantaneous value of the 2-Hz neural amplitude envelope (average stimulation rate) and the modeled oscillator phase (φ was estimated similarly to the behavioral analysis).

Dividing single-trial amplitudes into percentile bins allowed us to investigate relative amplitude changes while ignoring overall absolute magnitude differences across time points and participants (Ai and Ro, 2014; Cravo et al., 2013; Linkenkaer-Hansen et al., 2004). Overlapping bins were chosen to reduce noise in our data analysis (Cravo et al., 2013; Fiebelkorn et al., 2013; Henry et al., 2014). For each bin of the 15 × 15 grid, the proportion of correct responses (hit rate) was calculated, and subsequently averaged over the 0.03-s pre-target time points.

The 15 × 15 grid provides a full representation of the joint influences of delta-band neural amplitude and modeled oscillator phase on hit rates. To reduce complexity for the statistical analysis, hit rates were averaged across high 2-Hz amplitude bins (7 bins) and across low 2-Hz amplitude bins (7 bins) in order to test for performance modulations depending on neural amplitude variations. Similar to the analysis of the behavioral data, a quadratic function was fitted to the hit rates as a function of modeled oscillator phase, independently for high and low neural amplitudes. The estimated quadratic coefficients were subsequently tested against zero using a one-sample *t*-test (separately for high and low amplitudes) as well as compared against each other using a paired-samples *t*-test.

MEG data analysis: modulation of performance by neural amplitude in a wider time–frequency window

In a further analysis, we examined whether pre-target amplitude fluctuations at other neural frequencies and time points predicted the probability of detecting a target tone (intensity change). In detail, for each time–frequency bin (-0.3 to 0 s, 1–20 Hz), single-trial neural amplitudes were divided into 15 overlapping percentile bins (width: 30%) and hit rate was calculated for each bin. A quadratic function was fitted to the 15 hit rates as a function of amplitude percentile, independently for each time–frequency bin. For each participant, this resulted in one time–frequency representation (-0.3 to 0 s, 1–20 Hz) of estimated linear coefficients (i.e., the degree of linear modulation of hit rate by relative amplitude changes) and one time–frequency representation of estimated quadratic coefficients (i.e., the degree of quadratic modulation of hit rate by relative amplitude change).

Two separate one-sample *t*-tests were conducted for each time–frequency bin in order to test for linear and for quadratic modulation of hit rate by neural amplitude. The first tested the estimated linear coefficients against zero, the second tested the estimated quadratic coefficients against zero. This resulted in two time–frequency statistical maps containing p-values. A cluster extent threshold corrected for multiple comparisons at a level of $P \leq 0.05$ (Slotnick et al., 2003; Slotnick and Schacter, 2004). The cluster extent threshold was determined using a Monte Carlo simulation that was conducted independently for each of the two time–frequency statistical maps (linear coefficients; quadratic coefficients). In detail, p-values within each time–frequency statistical map were permuted 5000 times (i.e., shuffled across time–frequency bins) and the maximum cluster extent (entry threshold $P \leq 0.01$) on each permutation provided a distribution of maximum cluster extents in random data. The distribution of random cluster extents was then compared to the size of observed clusters (entry threshold $P \leq 0.01$), such that only those clusters that were larger than the 95th percentile of the permutation distribution were considered statistically significant.

MEG data analysis: low-frequency modulatory influences on linear/quadratic effects

In a final analysis, we examined whether low-frequency neural amplitude (2 Hz; delta band) has a modulatory influence on the linear or quadratic relationship between hit rate and neural amplitude observed in the analysis for each time–frequency bin (-0.3 to 0 s, 1–20 Hz). Low-frequency modulatory influences were independently investigated for each significant cluster.

In detail, for each time–frequency bin within a significant cluster, trials were sorted into a 15 × 15 grid of overlapping percentile bins (width: 30%) according to the high-frequency neural amplitudes (i.e., 7–9 Hz, 17–20 Hz, or 13–14 Hz; see Results) and the 2-Hz neural amplitudes at the same time point. For each bin of the 15 × 15 grid, the proportion of correct responses (hit rate) was calculated. Subsequently, the 15 × 15 hit-rate grids were averaged across time–frequency bins.

Modulatory influences of 2-Hz neural amplitude were then examined as follows. For significant linear clusters, a linear function was fitted to the 15 hit rates as a function of high-frequency amplitude (i.e., 7–9 Hz or 17–20 Hz; see Results), independently for each 2-Hz amplitude bin. Similarly, for significant quadratic clusters, a quadratic function was fitted to the 15 hit rates as a function high-frequency amplitude (i.e., 13–14 Hz; see Results), independently for each 2-Hz amplitude bin. This resulted in one linear/quadratic coefficient for each 2-Hz amplitude bin. Based on the distribution of the linear/quadratic coefficients as a function of 2-Hz amplitude (see Results), quadratic trend analyses were carried out in order to statistically test for 2-Hz modulatory influences. That is, a quadratic function was fitted either to the linear or quadratic coefficients as a function of 2-Hz amplitude, and estimated quadratic coefficients were subsequently tested against zero using a one-sample t-test, independently for each cluster.

Results

Human participants listened to temporally variable tone sequences (average onset-to-onset interval of 0.5 s = 2 Hz) and detected near-threshold target tones that were slightly louder in sound level than non-target tones (titrated for each individual; Fig. 2). Participants' average hit rate was 0.651 ($\pm$0.114 SD). The false alarm rate was 0.028 ($\pm$0.021 SD; calculated using the procedure described in Bendixen and Andersen, 2013). Here we investigated the extent to which temporal expectations in temporally variable sequences modulated target-detection performance as well as the association between detection performance and MEG-recorded pre-target neural amplitude states.

Behavioral data: modulation of perceptual performance by modeled oscillator phase

Each tone sequence exhibited temporal variability such that the temporal context leading up to a target tone varied. The degree to which each target was temporally expected was quantified as the phase of an oscillation estimated from a mathematical oscillator model (Large and Jones, 1999). Modeled phase values close to zero indicate good correspondence between the expected and the physical tone onset, while larger-magnitude values indicate that the tone onset would have been relatively unexpected (Fig. 2A).

Single-trials were sorted into 15 bins according to the modeled oscillator phase (Fig. 3A), and hit rate was calculated for each bin. The relationship between temporal expectations (modeled phase) and perceptual performance was assessed by means of a quadratic fit to hit rates as a function of modeled oscillator phase bins (Fig. 3B). Estimated quadratic coefficients were significantly smaller than zero ($t_{19} = -2.90$; P = 0.009, $r = 0.55$), indicating that hit rates were highest when the physical target onset coincided with the expected onset (i.e., the peak of the modeled oscillation), and lowest when target onset and expected onset diverged (Fig. 3C). We also examined whether the linear trend visible in Fig. 3C is statistically reliable by testing estimated linear coefficients (from our quadratic function fit) against zero. No significant difference was observed ($t_{19} = 1.48$, P = 0.154, $r = 0.322$).

Auditory cortex underlies delta-band (2-Hz) neural responses

The trial-averaged time-domain MEG signal was submitted to a fast Fourier transform (FFT), and the evoked amplitude spectrum was calculated (Fig. 4, left panel). The spectrum shows clear peaks at the average stimulation frequency (2 Hz) and its harmonics. Based on the complex coefficients from the fast Fourier transform at 2 Hz, a spatial filter was calculated which shows a typical auditory MEG topography (Fig. 4) and whose sources localize to auditory cortices (Fig. 4, middle panel; consistent with Herrmann et al., 2013). Single-trial time courses were projected through the spatial filter and thus reflect responses with the most likely sources in auditory cortex (i.e., a virtual source; de Cheveigné and Simon, 2008; Garrido et al., 2013), while other sources are suppressed. These spatially filtered single-trial time courses were used for all further analyses.

We then calculated the trial-averaged time-domain signal (time-locked to the target onset) for the auditory cortex virtual channel (i.e., after spatial filtering) for hit and miss trials (Fig. 4, top right panel). As expected, evoked neural responses in the post-target onset time interval (0.16–0.36 s) were larger for hits versus misses ($t_{19} = 2.95$, P = 0.008, $r = 0.56$; see also Ai and Ro, 2014; Gutschalk et al., 2008; Henry and Obleser, 2012; Snyder et al., 2015). Finally, an amplitude spectrum was calculated for each spatially filtered single-trial time-domain signal using a fast Fourier transform, and subsequently averaged across trials, showing a clear peak at 2 Hz (Fig. 4, bottom right panel). In subsequent analyses we focused on the association between behavioral performance and pre-target neural activity (and critically controlled that post-target onset activity variations would not affect pre-target neural amplitude effects, see Methods and materials).

Interactive influences of low-frequency neural amplitude and temporal expectations on performance

The amplitude of low-frequency neural oscillatory activity relates to the number of neurons exhibiting temporally synchronized activity and/or the strength of neural excitability fluctuations (Musall et al., 2014). Here we examined whether performance modulations by temporal expectations (modeled oscillator phase) are affected by low-frequency neural amplitude variations at target onset. To this end, single trials were sorted into a 15 × 15 grid according to the instantaneous 2-Hz neural amplitude directly prior to target onset (−0.03 to 0) and the modeled oscillator phase; hit rate was calculated for each bin of the grid (Fig. 5A).

For the statistical analysis, hit rates for high and low 2-Hz amplitude bins were averaged separately, and a quadratic function was fitted to the resulting hit rates as a function of binned modeled oscillator phase, independently for high and low 2-Hz amplitudes (Fig. 5B). The mean estimated quadratic coefficient was significantly different from zero for high 2-Hz amplitudes ($t_{19} = -4.92$, P < 0.001, $r = 0.75$) but not for low 2-Hz amplitudes ($t_{19} = -0.78$, P = 0.44, $r = 0.18$). A direct comparison of the mean quadratic coefficients between high and low 2-Hz amplitudes showed a stronger negative quadratic pattern for high than low 2-Hz amplitudes ($t_{19} = 2.76$, P = 0.012, $r = 0.54$; Fig. 5C). Thus, depending on the amplitude of the low-frequency (delta) neural oscillation, hit rates were weakly (low amplitude) or strongly (high amplitude) modulated by temporal expectations. Furthermore, mean hit rate across all oscillator phases did not differ between low and high amplitudes of the low-frequency oscillation ($t_{19} = 0.06$, P = 0.955, $r = 0.01$), and neither did optimal phase (i.e., the phase where performance was highest; $t_{19} = 0.38$, P = 0.707, $r = 0.077$). For qualitatively similar results using a 2 × 3 grid (amplitude: low, high × phase: early, on time, late) of non-overlapping bins see the Supplemental Materials and Figure S1.

We also confirmed the independence of modeled phase and pre-target 2-Hz neural amplitude (−0.03 to 0 s) by calculating the modulation of neural amplitude as a function of modeled oscillator phase using the same binning approach as before. Confirming theoretic assumptions, no linear ($t_{19} = 0.47$, P = 0.642, $r = 0.108$) or quadratic ($t_{19} = -0.25$, P = 0.804, $r = 0.058$) amplitude modulation was observed.
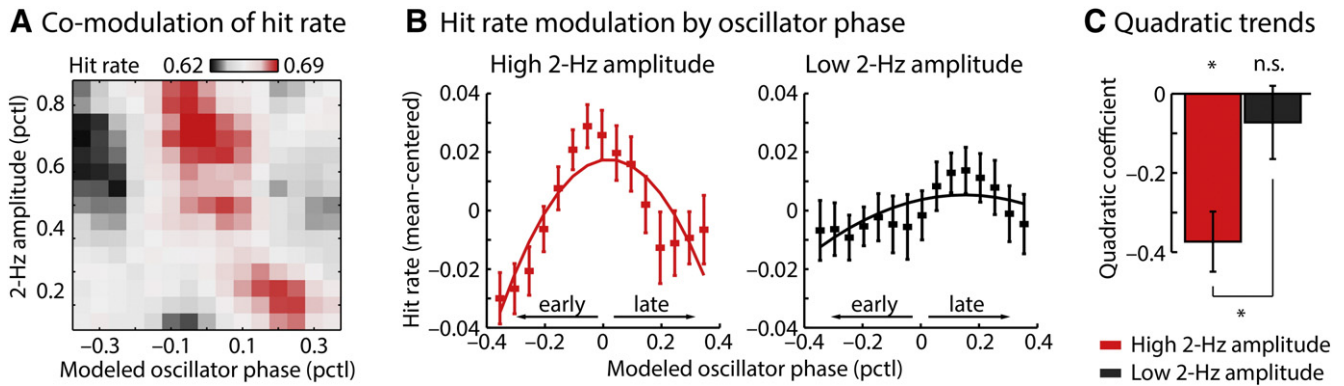
Fig. 5. Interactive influence of low-frequency neural amplitude (2 Hz) and temporal expectations (modeled oscillator phase) on performance. (A) Hit rate (average across participants) as a joint function of modeled oscillator phase (i.e., temporal expectation) and 2-Hz neural amplitude prior to target onset (−0.03 to 0 s); pctl — percentile. (B) Hit rates as a function of modeled oscillator phase bins for high and low 2-Hz neural amplitude (i.e., the average across high and low amplitude bins in panel A, respectively). A quadratic function was fitted to the hit rate data. (C) Mean quadratic coefficients from quadratic fits to the data in (B). Error bars reflect SEM. *P < 0.05, n.s. — not significant.

Modulation of perceptual performance by neural amplitude in a broader time–frequency window

Next, we examined whether pre-target neural amplitude fluctuations more broadly distributed in time and frequency predict perceptual performance (−0.3 to 0 s; 1–20 Hz). At each time–frequency bin, single trials were sorted into 15 bins according to the neural amplitude, and hit rate was calculated for each bin. A quadratic function was fitted to hit rates as a function of binned neural amplitude, and the estimated linear and quadratic coefficients were extracted.

Examining the linear relationship between neural amplitude and hit rates (linear coefficient tested against zero) revealed two significant clusters for which hit rates increased with increasing neural amplitude (Fig. 6A). The first cluster was observed at around −0.15 to −0.03 s pre-target onset in the 7–9 Hz (alpha; Lehtelä et al., 1997) frequency range. The second cluster was observed at around −0.1 to −0.05 s pre-target onset in the 17–20 Hz (beta) frequency range. The individual linear trends for each cluster are displayed in Fig. 6B.

Examining the quadratic relation between neural amplitude and hit rates (quadratic coefficient tested against zero) revealed one significant

cluster at around −0.275 to −0.225 s pre-target onset in the 13–14 Hz (alpha) frequency range (Fig. 6A). For this cluster, hit rates were largest when neural amplitude was low or high, while hit rates were lowest for intermediate neural amplitudes (Fig. 6B).

Note that in Fig. 6 there is no simple (i.e., direct) linear or quadratic effect of 2-Hz neural amplitude on detection performance due to the complex interaction pattern with temporal expectations (modeled oscillator phase). That is, for early and late targets, hit rates decreased with increasing 2-Hz amplitude, while for on-time targets, the pattern was reversed (Fig. 5A).

Low-frequency (delta) neural amplitude modulates linear and quadratic performance effects

Next, we examined whether 2-Hz neural amplitude has a modulatory influence on the linear and quadratic neural amplitude-to-hit rate relations observed in the overall analysis for each time–frequency bin (see previous section and Fig. 6).

In detail, for both linear clusters, we investigated the influences of high-frequency (alpha/beta) neural amplitude (7–9 Hz; 17–20 Hz) on
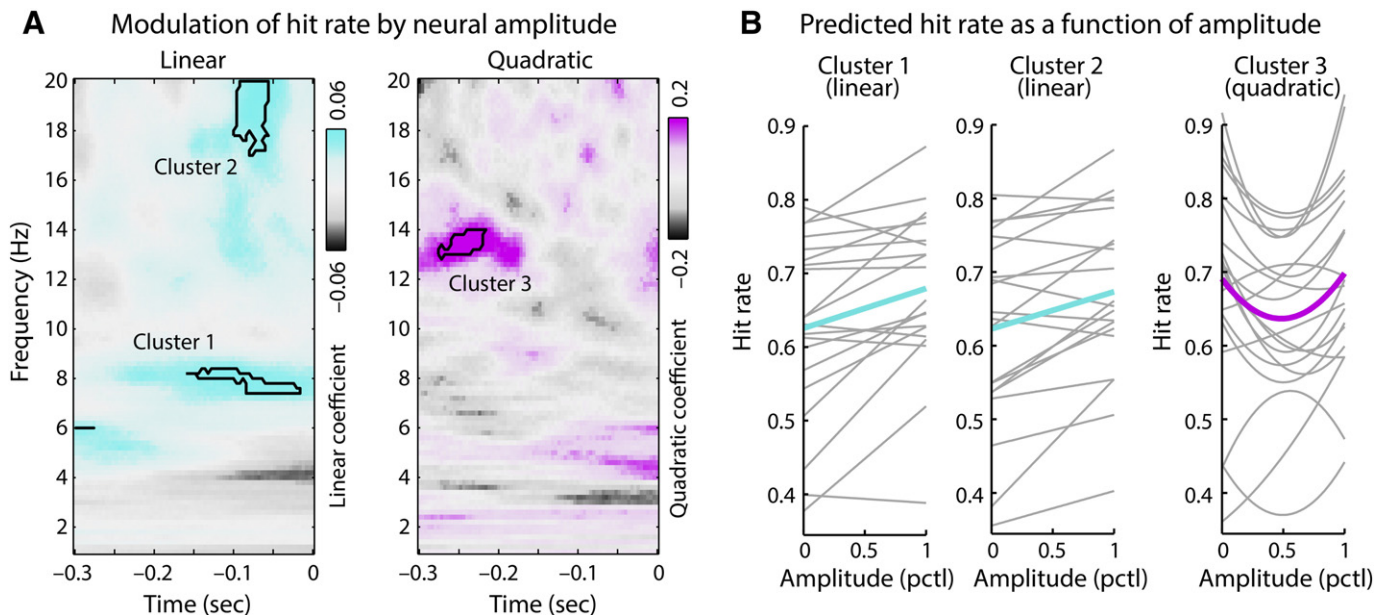

Fig. 6. Influence of pre-target neural amplitude on performance. (A) Linear (left, cyan) and quadratic (right, magenta) coefficients from quadratic fits to hit rates as a function bin neural amplitude, separately for each time–frequency bin. Significant clusters, that is, where the linear/quadratic coefficients are significantly different from zero, are outlined in black (i.e., modulation of hit rates by neural amplitude). (B) Predicted hit rates for the significant clusters in (A). Individual fits are displayed in gray and the average across participants in color. pctl — percentiles.

hit rate for different magnitudes of the low-frequency (2 Hz) neural responses (Fig. 7). That is, single trials were sorted into a 15×15 grid according to the 2-Hz neural amplitude and the high-frequency neural amplitude (alpha/beta). Hit rate was calculated for each grid bin, and a linear function was fitted to hit rates as a function of high-frequency neural amplitude, separately for each 2-Hz amplitude bin. Modulation of linear coefficients by 2-Hz amplitude was tested statistically by fitting a quadratic function to the linear coefficients and testing the resulting quadratic coefficient against zero. For neither cluster (7–9 Hz and 17–20 Hz) were the quadratic coefficients significantly different from zero (7–9 Hz: $t_{19} = -1.59$, $P = 0.127$, $r = 0.34$; 17–20 Hz: $t_{19} = 0.33$, $P = 0.747$, $r = 0.08$). However, the presence of a 2-Hz modulatory effect on the 7–9 Hz cluster (which is apparent visually in Fig. 7B and C) was confirmed by a significant dependent samples t-test testing the mean linear coefficients across the two bins with lowest 2-Hz amplitude and the two bins with highest 2-Hz amplitude against the mean linear coefficients across three intermediate bins (0.55–0.65 pctl; $t_{19} = 3.02$, $P = 0.007$, $r = 0.57$). Hit rates most strongly decreased with decreasing alpha amplitude (7–9 Hz) when the amplitude of the delta response (2 Hz) was intermediate.

Finally, we examined low-frequency (2 Hz) amplitude influences on the quadratic relation between 13–14 Hz (alpha) neural amplitude and hit rates (Fig. 8). That is, single trials were sorted into a 15×15 grid according to the 2-Hz neural amplitude and the 13–14-Hz neural amplitude, and a quadratic function was fitted to hit rates (that were calculated for each grid bin) as a function of 13–14-Hz amplitude, separately for each 2-Hz amplitude bin. The 2-Hz modulatory influences were statistically tested using a quadratic trend analysis on quadratic coefficients (Fig. 8B). The mean estimated quadratic coefficient was significantly larger than zero ($t_{19} = 2.88$, $P = 0.01$, $r = 0.55$), thus showing a positive quadratic trend. In other words, target detection performance was best when low-frequency amplitude and high-frequency amplitude were simultaneously high or low. Intermediate neural amplitudes simultaneously in both frequency bands, however, showed lowest detection performance.

Note that modulation of perceptual performance by the modeled oscillator phase (temporal expectations) was not modulated by amplitude (low versus high) in any of the three alpha/beta clusters (comparison of

quadratic coefficients for low versus high alpha/beta amplitude, similarly calculated as for 2-Hz neural activity; for all, $P > 0.30$).

Discussion

The current MEG study investigated the joint influence of temporal expectations and neural amplitude on target detection performance. The results were as follows: (i) Detection performance was highest for expected events in temporally-variable sequences; (ii) Modulation of
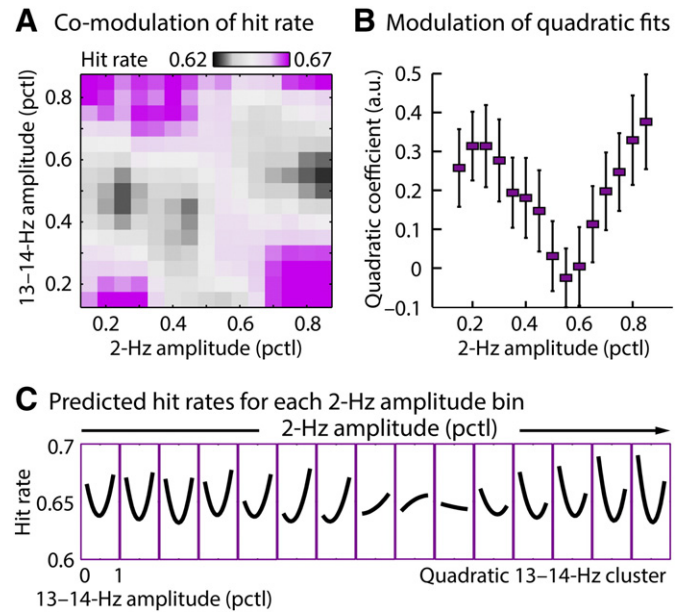

Fig. 8. Modulatory influences of low-frequency amplitudes on quadratic 13–14 Hz effects. (A) Hit rates as a joint function of 13–14-Hz amplitude and 2-Hz amplitude (pctl — percentile). (B) Quadratic coefficients from fits to hit rates as a function of 13–14-Hz amplitude for each 2-Hz amplitude bin. Error bars reflect SEM. (C) Predicted hit rates for each 2-Hz amplitude bin.
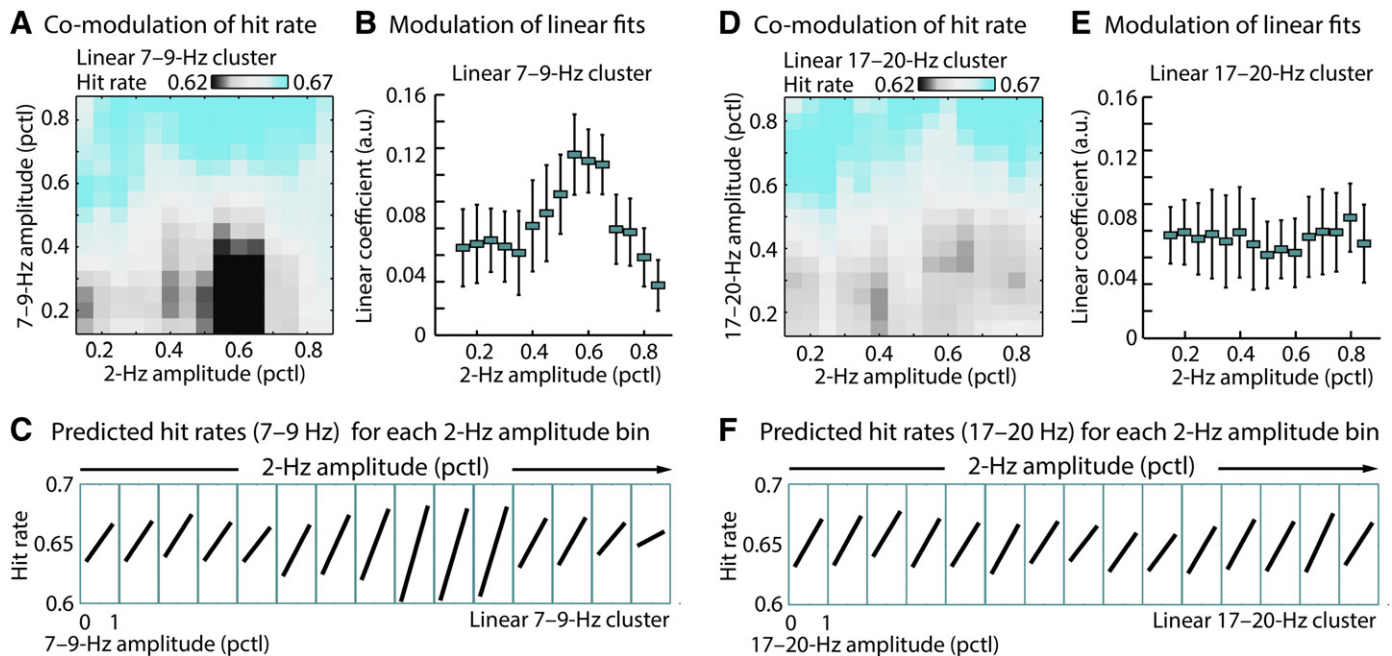

Fig. 7. Modulatory influences of low-frequency amplitudes on linear 7–9 Hz and 17–20 Hz effects. (A) Hit rates as a joint function of 7–9-Hz amplitude and 2-Hz amplitude (pctl — percentile). (B) Linear coefficients from fitting a linear function to hit rates as a function of 7–9-Hz amplitude for each 2-Hz amplitude bin. Error bars reflect SEM. (C) Predicted hit rates for each 2-Hz amplitude bin. (D–F) Similar to (A–C) for the linear 17–20 Hz cluster.

performance by temporal expectations was affected by low-frequency (delta-band) amplitude; (ii) Alpha- and beta-band neural amplitude linearly and quadratically modulated performance, and these relations were in turn modulated by delta-band neural amplitude. Thus, the current study shows that temporal expectations and neural amplitude fluctuations interactively influence perceptual performance, and further that performance is linearly and nonlinearly affected by complex interactions between multiple neural frequency bands.

Temporal expectations affect perceptual performance in temporally variable sequences

Detection of near-threshold intensity changes was best when the timing of targets was consistent with temporal expectations. Our observation is in line with previous studies manipulating either the timing of targets or the timing of a whole sequence (Barnes and Jones, 2000; Jones et al., 2002, 2006; Mathewson et al., 2012; Rohenkohl et al., 2012). Importantly, our results show that subtle variations in the degree of temporal expectation also affect perceptual performance in temporally variable sequences (see also Jones and Yee, 1997).

Temporal expectations were quantified as the phase of a modeled oscillation (Large and Jones, 1999; McAuley and Jones, 2003), in line with recent theoretical and empirical advances suggesting that the phase of low-frequency neural oscillations reflects a biophysical substrate of temporal expectations (Henry and Herrmann, 2014; Large, 2008; Schroeder and Lakatos, 2009b). Hence, the modulation of performance by the modeled oscillator phase (temporal expectations) is also in line with previous reports of performance modulations by the neural phase of entrained low-frequency oscillations (Cravo et al., 2013; Henry et al., 2014; Henry and Obleser, 2012; Neuling et al., 2012; Stefanics et al., 2010).

Low-frequency neural amplitude variations influence performance modulation by temporal expectations

Temporal expectation (i.e., modeled oscillator phase) affected performance only for high but not for low amplitudes of the delta neural oscillation in auditory cortex. On the level of single- or multi-unit activity, delta oscillations reflect fluctuations in excitability (Bishop, 1933; Lakatos et al., 2005), with the oscillations' amplitude reflecting the strength of the excitability fluctuations (Fig. 1, Jensen and Mazaheri, 2010). In MEG recordings, low-frequency oscillatory amplitude is additionally influenced by the number of neurons exhibiting synchronized excitability fluctuations, because neural activity measured at the scalp reflects the summed activity of many responding neurons (Musall et al., 2014). Consequently, MEG delta-band amplitude is related to the strength of excitability fluctuations as well as to the temporal synchrony of these fluctuations between neurons, and both, in the context of rhythmic stimulation, might be affected by the level of synchronization of neural oscillations with external events (Thut et al., 2011). The observed relation between perceptual performance and temporal expectations (modeled oscillator phase) is thus consistent with neural dynamics: Perceptual performance is only modulated when neural excitability fluctuations and/or temporal synchrony between neurons are large (high amplitude).

Performance modulation by (neural) oscillatory phase for high but not for low neural amplitudes has also been observed for alpha oscillations (Mathewson et al., 2009). Our approach, however, avoids the possibility of poor neural phase estimation for low neural amplitude values (Muthukumaraswamy and Singh, 2011) by estimating oscillatory phase using a model from established behavioral research (Large and Jones, 1999). Thus, we can be confident that this finding reflects a fundamental difference between low and high 2-Hz amplitude rather than reflecting an inability to measure neural phase when neural amplitude is low.

Furthermore, overall performance did not differ between low and high amplitudes of the low-frequency (delta) oscillation. This observation can be related to the (a)symmetry of 2-Hz neural excitability fluctuations. Consider for example alpha (and sometimes beta; Weisz et al., 2010) oscillations, which are thought to reflect asymmetric excitability fluctuations (Jensen and Mazaheri, 2010; Klimesch et al., 2007; Mathewson et al., 2011). When the strength of excitability fluctuations increases (i.e., when alpha/beta amplitude is high), neural populations exhibit longer periods of low excitability and thus inhibition, resulting in overall decreased performance compared to when alpha/beta amplitude is low (Bonnefond and Jensen, 2012; Capilla et al., 2014; Haegens et al., 2011a; van Ede et al., 2011). In contrast, the absence of a performance difference here between low and high delta amplitude speaks against such asymmetry for low-frequency oscillations, but instead is more consistent with symmetrical delta-band neural excitability levels.

Linear relation between alpha/beta-band activity and perceptual performance

We also observed a positive linear relation between pre-target neural alpha/beta-band activity in auditory cortex and performance (Fig. 6). Most previous studies investigating alpha- and beta-band amplitude focused on posterior or somatosensory cortices (Capilla et al., 2014; Haegens et al., 2011b; Jensen and Mazaheri, 2010; van Ede et al., 2011). In the auditory domain, evidence for alpha/beta-band effects is sparse (but see Frey et al., 2014; Lehtelä et al., 1997; Müller et al., in press; for a review see Weisz and Obleser, 2014) and our study thus provides important evidence that alpha- and beta-band activity in auditory cortex affects perceptual performance.

However, the direction of our observed effects is in contrast to previous observations. That is, previous studies observed a negative linear relation between alpha/beta amplitude and performance (Capilla et al., 2014; van Dijk et al., 2008), which has been related to asymmetric excitability fluctuations and consequently to neural inhibition (see previous section, Jensen and Mazaheri, 2010). Our observation of a positive linear relation is inconsistent with this neural inhibition framework. Nevertheless, there are reports of a positive linear relation similar to our findings (Arnal et al., 2015; Haegens et al., 2014; Jones et al., 2010). In addition, alpha oscillations in the temporal cortex maintain an opposite relationship to behavioral performance and spiking output than alpha oscillations in visual cortices (Bollimunta et al., 2008; Mo et al., 2011) in line with distributed alpha systems in the brain (Başar et al., 1997). These results, together with observed nonlinear relations between alpha/beta amplitude and behavior (Ai and Ro, 2014; Linkenkaer-Hansen et al., 2004; Zhang and Ding, 2010), tentatively suggest that neural inhibition associated with alpha/beta-band oscillations is not a universal phenomenon (Palva and Palva, 2007, 2011). The positive linear alpha/beta-band effects in the current study might reflect an increase in oscillatory synchronization between neural populations at alpha and beta frequency just prior to detected targets. In particular for the beta band, bursts of synchronous activity have been related to anticipation during rhythm perception (Arnal et al., 2015; Fujioka et al., 2012; Large and Snyder, 2009; Saleh et al., 2010).

Quadratic modulation of performance by neural amplitude in multiple frequency bands

We also observed a positive quadratic modulation of perceptual performance in the alpha frequency band. Furthermore, delta-band (2 Hz) activity modulated both the linear and quadratic effects in the alpha band in a quadratic fashion. The linear performance decrease with decreasing alpha amplitude was strongest at intermediate delta amplitudes, and the quadratic modulation of performance in the alpha-band was weakest at intermediate delta amplitudes.

Our findings are consistent with a theoretical perspective that places complex neural interactions at the center of brain and cognitive function (Breakspear, 2004; Buzsaki, 2006; Kayser et al., 2015; Stam, 2005;

Thut et al., 2012; Womelsdorf et al., 2014). Specifically, effects of cross-frequency relations on performance have recently been observed for phase–phase interactions (Fiebelkorn et al., 2013; Henry et al., 2014), phase–amplitude coupling (Arnal et al., 2015; Friese et al., 2013), and power–power coupling (Mazaheri et al., 2009). An important distinction between the current study and previous studies (but see Henry et al., 2014) is that our analysis does not rely on a nested relationship between low- and high-frequency oscillations, but instead shows that coincidental (i.e., nested or non-nested) amplitude fluctuations in multiple frequency bands affect performance. Investigation of coincidental neural dynamics might therefore reveal complex relations between multiple frequency bands hidden in or different from investigations of systematic, coupled fluctuations across neural frequencies.

Critically, in the current data, performance was relatively good for both low and high values of alpha and delta amplitude, while performance was relatively poor for intermediate amplitude values (Fig. 8). A speculative interpretation of the data is that the quadratic modulations of performance might be a signature of shifts between states in which the current listening task could be solved. In particular in the context of temporally variable sequences like those examined here, a pre-target high-delta state might reflect a successful integration of preceding temporal context using a "rhythmic" processing mode (Lakatos et al., 2008). On the other hand, a pre-target low-delta state might reflect a different, more "continuous" processing mode after failure to integrate the previous temporal context (Henry and Herrmann, 2012; Schroeder and Lakatos, 2009a). In contrast to shifts in states induced by external event structure (affecting the delta band), alpha-band activity might be related to more internal, non-stimulus-driven attentional processes, perhaps related to the time scale of attention. One strategy (associated with low alpha amplitudes) might be to focus locally and shift attention between individual tones to monitor for intensity deviants. On the other hand, a more global (high alpha) strategy would involve directing attention to the sequence level. Importantly, different states support perceptual performance, while intermediate delta and alpha levels might reflect a metabolically relatively expensive transition period between the states (Stam, 2005). Although this interpretation is speculative and needs further examination, the current findings point towards complex nonlinear dynamics of neural activity affecting listening performance.

Conclusion

The current MEG study investigated the interaction of temporal expectations in temporally variable sequences and neural amplitude variations in auditory cortex on listening performance. We show that performance modulations by temporal expectations are only observed when pre-target neural amplitude is high. In addition, performance is linearly and nonlinearly modulated by pre-target alpha-band activity and linearly modulated by beta-band activity. Effects of alpha activity on behavior were further modulated by low-frequency neural activity in the delta band. Thus, complex interactions of temporal expectations and neural activity in multiple frequency bands influence perceptual performance in a temporally variable context.

Acknowledgments

Appendix A. Supplementary data

Supplementary data to this article can be found online at http://dx.doi.org/10.1016/j.neuroimage.2015.09.019.

References

Ai, L., Ro, T., 2014. The phase of prestimulus alpha oscillations affects tactile perception. J. Neurophysiol. 111, 1300–1307.
Ali, M.M., Sellers, K.K., Fröhlich, F., 2013. Transcranial alternating current stimulation modulates large-scale cortical network activity by network resonance. J. Neurosci. 33, 11262–11275.
Arnal, L.H., Giraud, A.-L., 2012. Cortical oscillations and sensory predictions. Trends Cogn. Sci. 16, 390–398.
Arnal, L.H., Doelling, K.B., Poeppel, D., 2015. Delta-beta coupled oscillations underlie temporal prediction accuracy. Cereb. Cortex 25, 3077–3085.
Barnes, R., Jones, M.R., 2000. Expectancy, attention, and time. Cogn. Psychol. 41, 254–311.
Başar, E., Schürmann, M., Başar-Eroglu, C., Karakaş, S., 1997. Alpha oscillations in brain functioning: an integrative theory. Int. J. Psychophysiol. 26, 5–29.
Bell, A.J., Sejnowski, T.J., 1995. An information maximization approach to blind separation and blind deconvolution. Neural Comput. 7, 1129–1159.
Bendixen, A., Andersen, S.K., 2013. Measuring target detection performance in paradigms with high event rates. Clin. Neurophysiol. 124, 928–940.
Besl, P.J., McKay, N.D., 1992. A method for registration of 3-D shapes. IEEE Trans. Pattern Anal. Mach. Intell. 14, 239–256.
Besle, J., Schevon, C.A., Mehta, A.D., Lakatos, P., Goodman, R.R., McKhann, G.M., Emerson, R.G., Schroeder, C.E., 2011. Tuning of the human neocortex to the temporal dynamics of attended events. J. Neurosci. 31, 3176–3185.
Bishop, G.H., 1933. Cyclic changes in excitability of the optic pathway of the rabbit. Am. J. Physiol. 103, 213–224.
Bollimunta, A., Cheng, Y., Schroeder, C.E., Ding, M., 2008. Neuronal mechanisms of cortical alpha oscillations in awake-behaving macaques. J. Neurosci. 28, 9976–9988.
Bonnefond, M., Jensen, O., 2012. Alpha oscillations serve to protect working memory maintenance against anticipated distracters. Curr. Biol. 22, 1969–1974.
Breakspear, M., 2004. "Dynamic" connectivity in neural systems. Neuroinformatics 2, 205–226.
Busch, N.A., VanRullen, R., 2010. Spontaneous EEG oscillations reveal periodic sampling of visual attention. Proc. Natl. Acad. Sci. 107, 16048–16053.
Busch, N.A., Dubois, J., VanRullen, R., 2009. The phase of ongoing EEG oscillations predicts visual perception. J. Neurosci. 29, 7869–7876.
Buzsaki, G., 2006. Rhythms of the Brain. Oxford University Press, New York, USA.
Canavier, C.C., 2015. Phase-resetting as a tool of information transmission. Curr. Opin. Neurobiol. 31, 206–213.
Capilla, A., Schoffelen, J.-M., Paterson, G., Thut, G., Gross, J., 2014. Dissociated α-band modulations in the dorsal and ventral visual pathways in visuospatial attention and perception. Cereb. Cortex 24, 550–561.
Cravo, A.M., Rohenkohl, G., Wyart, V., Nobre, A.C., 2013. Temporal expectation enhances contrast sensitivity by phase entrainment of low-frequency oscillations in visual cortex. J. Neurosci. 33, 4002–4010.
de Cheveigné, A., Simon, J.Z., 2008. Denoising based on spatial filtering. J. Neurosci. Methods 171, 331–339.
Fiebelkorn, I.C., Snyder, A.C., Mercier, M.R., Butler, J.S., Molholm, S., Foxe, J.J., 2013. Cortical cross–frequency coupling predicts perceptual outcomes. NeuroImage 69, 126–137.
Fischl, B., Sereno, M.I., Dale, A.M., 1999a. Cortical surface-based analysis II: inflation, flattening, and a surface-based coordinate system. NeuroImage 9, 195–207.
Fischl, B., Sereno, M.I., Tootell, R.B.H., Dale, A.M., 1999b. High-resolution intersubject averaging and a coordinate system for the cortical surface. Hum. Brain Mapp. 8, 272–284.
Frey, J.N., Mainy, N., Lauchaux, J.-P., Müller, N., Bertrand, O., Weisz, N., 2014. Selective modulation of auditory cortical alpha activity in an audiovisual spatial attention task. J. Neurosci. 34, 6634–6639.
Friese, U., Köster, M., Hassler, U., Martens, U., Trujillo-Barreto, N.J., Gruber, T., 2013. Successful memory encoding is associated with increased cross–frequency coupling between frontal theta and posterior gamma oscillations in human scalp-recorded EEG. NeuroImage 66, 642–647.
Fröhlich, F., McCormick, D.A., 2010. Endogenous electric fields may guide neocortical network activity. Neuron 67, 129–143.
Fujioka, T., Trainor, L.J., Large, E.W., Ross, B., 2012. Internalized timing of isochronous sounds is represented in neuromagnetic beta oscillations. J. Neurosci. 32, 1791–1802.
Garrido, M.I., Sahani, M., Dolan, R.J., 2013. Outlier responses reflect sensitivity to statistical structure in the human brain. PLoS Comput. Biol. 9, e1002999.
Giraud, A.-L., Poeppel, D., 2012. Cortical oscillations and speech processing: emerging computational principles and operations. Nat. Neurosci. 15.
Gross, J., Kujala, J., Hämäläinen, M.S., Timmermann, L., Schnitzler, A., Salmelin, R., 2001. Dynamic imaging of coherent sources: studying neural interactions in the human brain. Proc. Natl. Acad. Sci. 98, 694–699.
Gutschalk, A., Michey, C., Oxenham, A.J., 2008. Neural correlates of auditory perceptual awareness under informational masking. PLoS Biol. 6, e138.
Haegens, S., Händel, B.F., Jensen, O., 2011a. Top-down controlled alpha band activity in somatosensory areas determines behavioral performance in a discrimination task. J. Neurosci. 31, 5197–5204.
Haegens, S., Nácher, V., Luna, R., Romo, R., Jensen, O., 2011b. α-Oscillations in the monkey sensorimotor network influence discrimination performance by rhythmical inhibition of neuronal spiking. Proc. Natl. Acad. Sci. 108, 19377–19382.
Haegens, S., Vázquez, Y., Zainos, A., Alvarez, M., Jensen, O., Romo, R., 2014. Thalamocortical rhythms during a vibrotactile detection task. Proc. Natl. Acad. Sci. 111, 1797–1805.
Hämäläinen, M.S., Hari, R., Ilmoniemi, R.J., Knuutila, J., Lounasmaa, O.V., 1993. Magnetoencephalography — theory, instrumentation, and applications to noninvasive studies of the working human brain. Rev. Mod. Phys. 65, 413–497.
Han, X., Jovicich, J., Salat, D.H., van der Kouwe, A., Quinn, B., Czanner, S., Busa, E., Pacheco, J., Albert, M., Killiany, R., Maguire, P., Rosas, D., Makris, N., Dale, A.M., Dickerson, B.,

Fischl, B.R., 2006. Reliability of MRI-derived measurements of human cerebral cortical thickness: the effects of field strength, scanner upgrade and manufacturer. NeuroImage 32, 180–194.

Hanslmayr, S., Volberg, G., Wimber, M., Dalal, S.S., Greenlee, M.W., 2013. Prestimulus oscillatory phase at 7 Hz gates cortical information flow and visual perception. Curr. Biol. 23, 2273–2278.

Henry, M.J., Herrmann, B., 2012. A precluding role of low-frequency oscillations for auditory perception in a continuous processing mode. J. Neurosci. 32, 17525–17527.

Henry, M.J., Herrmann, B., 2014. Low-frequency neural oscillations support dynamic attending in temporal context. Timing & Time Perception. 2 pp. 62–86.

Henry, M.J., Obleser, J., 2012. Frequency modulation entrains slow neural oscillations and optimizes human listening behavior. Proc. Natl. Acad. Sci. 109, 20095–20100.

Henry, M.J., Herrmann, B., Obleser, J., 2014. Entrained neural oscillations in multiple frequency bands co-modulate behavior. Proc. Natl. Acad. Sci. 111, 14935–14940.

Herrmann, B., Henry, M.J., Grigutsch, M., Obleser, J., 2013. Oscillatory phase dynamics in neural entrainment underpin illusory percepts of time. J. Neurosci. 33, 15799–15809.

Inden, B., Malisz, Z., Wagner, P., Wachsmuth, I., 2012. Rapid entrainment to spontaneous speech: a comparison of oscillator models. In: Miyake, N., Peebles, D., Cooper, R.P. (Eds.), 34th Annual Conference of the Cognitive Science Society. Cognitive Science Society, Sapporo, Japan.

Jensen, O., Mazaheri, A., 2010. Shaping functional architecture by oscillatory alpha activity: gating by inhibition. Front. Hum. Neurosci. 4, 186.

Jones, M.R., Boltz, M.G., 1989. Dynamic attending and responses to time. Psychol. Rev. 96, 459–491.

Jones, M.R., Yee, W., 1997. Sensitivity to time change: the role of context and skill. J. Exp. Psychol. Hum. Percept. Perform. 23, 693–709.

Jones, M.R., Moynihan, H., MacKenzie, N., Puente, J., 2002. Temporal aspects of stimulus-driven attending in dynamic arrays. Psychol. Sci. 13, 313–319.

Jones, M.R., Johnston, H.M., Puente, J., 2006. Effects of auditory pattern structure on anticipatory and reactive attending. Cogn. Psychol. 53, 59–96.

Jones, S.R., Kerr, C.E., Wan, Q., Pritchett, D.L., Hämäläinen, M.S., Moore, C.I., 2010. Cued spatial attention drives functionally relevant modulation of the mu rhythm in primary somatosensory cortex. J. Neurosci. 30, 13760–13765.

Kayser, C., Wilson, C., Safaai, H., Sakata, S., Panzeri, S., 2015. Rhythmic auditory cortex activity at multiple timescales shapes stimulus-response gain and background firing. J. Neurosci. 35, 7750–7762.

Klimesch, W., Sauseng, P., Hanslmayr, S., 2007. EEG alpha oscillations: the inhibition–timing hypothesis. Brain Res. Rev. 53, 63–88.

Lakatos, P., Shah, A.S., Knuth, K.H., Ulbert, I., Karmos, G., Schroeder, C.E., 2005. An oscillatory hierarchy controlling neuronal excitability and stimulus processing in the auditory cortex. J. Neurophysiol. 94, 1904–1911.

Lakatos, P., Karmos, G., Mehta, A.D., Ulbert, I., Schroeder, C.E., 2008. Entrainment of neuronal oscillations as a mechanism of attentional selection. Science 320, 110–113.

Lakatos, P., Musacchia, G., O'Connel, M.N., Falchier, A.Y., Javitt, D.C., Schroeder, C.E., 2013. The spectrotemporal filter mechanism of auditory selective attention. Neuron 77, 750–761.

Lange, K., 2009. Brain correlates of early auditory processing are attenuated by expectations for time and pitch. Brain Cogn. 69, 127–137.

Large, E.W., 2008. Resonating to musical rhythm: theory and experiment. In: Grondin, S. (Ed.), Psychology of Time. Emerald Group, Bingley, UK, pp. 189–232.

Large, E.W., Jones, M.R., 1999. The dynamics of attending: how people track time-varying events. Psychol. Rev. 106, 119–159.

Large, E.W., Snyder, J.S., 2009. Pulse and meter as neural resonance. Ann. N. Y. Acad. Sci. 1169, 46–57.

Lawrance, E.L.A., Harper, N.S., Cooke, J.E., Schnupp, J.W.H., 2014. Temporal predictability enhances auditory detection. J. Acoust. Soc. Am. 136, EL357–EL363.

Lehtelä, L., Salmelin, R., Hari, R., 1997. Evidence for reactive magnetic 10-Hz rhythm in the human auditory cortex. Neurosci. Lett. 222, 111–114.

Linkenkaer-Hansen, K., Nikulin, V.V., Palva, S., Ilmoniemi, R.J., Palva, J.M., 2004. Prestimulus oscillations enhance psychophysical performance in humans. J. Neurosci. 24, 10186–10190.

Makeig, S., Bell, A.J., Jung, T.-P., Sejnowski, T.J., 1996. Independent component analysis of electroencephalographic data. In: Touretzky, D., Mozer, M., Hasselmo, M. (Eds.), Advances in Neural Information Processing Systems. MIT Press, Cambridge, MA, USA.

Mathewson, K.E., Gratton, G., Fabiani, M., Beck, D.M., Ro, T., 2009. To see or not to see: prestimulus phase predicts visual awareness. J. Neurosci. 29, 2725–2732.

Mathewson, K.E., Lleras, A., Beck, D.M., Fabiani, M., Ro, T., Gratton, G., 2011. Pulsed out of awareness: EEG alpha oscillations represent a pulsed-inhibition of ongoing cortical processing. Front. Psychol. 2, 99.

Mathewson, K.E., Prudhomme, C., Fabiani, M., Beck, D.M., Lleras, A., Gratton, G., 2012. Making waves in the stream of consciousness: entraining oscillations in EEG alpha and fluctuations in visual awareness with rhythmic visual stimulation. J. Cogn. Neurosci. 24, 2321–2333.

Mazaheri, A., Nieuwenhuis, I.L., van Dijk, H., Jensen, O., 2009. Prestimulus alpha and mu activity predicts failure to inhibit motor responses. Hum. Brain Mapp. 30, 1791–1800.

McAuley, J.D., Jones, M.R., 2003. Modeling effects of rhythmic context on perceived duration: a comparison of interval and entrainment approaches to short-interval timing. J. Exp. Psychol. Hum. Percept. Perform. 29, 1102–1125.

Mo, J., Schroeder, C.E., Ding, M., 2011. Attentional modulation of alpha oscillations in macaque inferotemporal cortex. J. Neurosci. 31, 878–882.

Monto, S., Palva, S., Voipio, J., Palva, J.M., 2008. Very slow EEG fluctuations predict the dynamics of stimulus detection and oscillation amplitudes in humans. J. Neurosci. 28, 8268–8272.

Müller, N., Leske, S., Hartmann, T., Szebényi, S., Weisz, N., 2015. Listen to yourself: the medial prefrontal cortex modulates auditory alpha power during speech preparation. Cereb. Cortex (in press).

Musall, S., von Pföstl, V., Rauch, A., Logothetis, N.K., Whittingstall, K., 2014. Effects of neural synchrony on surface EEG. Cereb. Cortex 24.

Muthukumaraswamy, S.D., Singh, K.D., 2011. A cautionary note on the interpretation of phase-locking estimates with concurrent changes in power. Clin. Neurophysiol. 122, 2324–2325.

Neuling, T., Rach, S., Wagner, S., Wolters, C.H., Herrmann, C.S., 2012. Good vibrations: oscillatory phase shapes perception. NeuroImage 63, 771–778.

Ng, B.S.W., Schroeder, T., Kayser, C., 2012. A precluding but not ensuring role of entrained low-frequency oscillations for auditory perception. J. Neurosci. 32, 12268–12276.

Nitschke, J.B., Miller, G.A., Cook III, E.W., 1998. Digital filtering in EEG/ERP analysis: some technical and empirical comparisons. Behav. Res. Methods Instrum. Comput. 30, 54–67.

Nolte, G., 2003. The magnetic lead field theorem in the quasi-static approximation and its use for magnetoencephalography forward calculation in realistic volume conductors. Phys. Med. Biol. 48, 3637–3652.

O'Connel, M.N., Barczak, A., Schroeder, C.E., Lakatos, P., 2014. Layer specific sharpening of frequency tuning by selective attention in primary auditory cortex. J. Neurosci. 34, 16496–16508.

Oostenveld, R., Fries, P., Maris, E., Schoffelen, J.M., 2011. FieldTrip: open source software for advanced analysis of MEG, EEG, and invasive electrophysiological data. Comput. Intell. Neurosci. 2011, 156869.

Palva, S., Palva, J.M., 2007. New vistas for alpha-frequency band oscillations. Trends Neurosci. 30, 150–158.

Palva, S., Palva, J.M., 2011. Functional roles of alpha-band phase synchronization in local and large-scale cortical networks. Front. Psychol. 2, 204.

Pascual-Marqui, R.D., 2002. Standardized low resolution brain electromagnetic tomography (sLORTEA): technical details. Methods Find. Exp. Clin. Pharmacol. 24, 5–12.

Peelle, J.E., Davis, M.H., 2013. Neural oscillations carry speech rhythm through to comprehension. Front. Psychol. 3, 320.

Rohenkohl, G., Nobre, A.C., 2011. Alpha oscillations related to anticipatory attention follow temporal expectations. J. Neurosci. 31, 14076–14084.

Rohenkohl, G., Cravo, A.M., Wyart, V., Nobre, A.C., 2012. Temporal expectation improves the quality of sensory information. J. Neurosci. 32, 8424–8428.

Rosenthal, R., Rubin, D.B., 2003. $r_{equivalent}$: a simple effect size indicator. Psychol. Methods 8, 492–496.

Saleh, M., Reimer, J., Penn, R., Ojakangas, C.L., Hatsopoulos, N.G., 2010. Fast and slow oscillations in human primary motor cortex predict oncoming behaviorally relevant cues. Neuron 65, 461–471.

Schroeder, C.E., Lakatos, P., 2009a. The gamma oscillation: master or slave? Brain Topogr. 22, 24–26.

Schroeder, C.E., Lakatos, P., 2009b. Low-frequency neuronal oscillations as instruments of sensory selection. Trends Neurosci. 32, 9–18.

Slotnick, S.D., Schacter, D.L., 2004. A sensory signature that distinguishes true from false memories. Nat. Neurosci. 7, 664–672.

Slotnick, S.D., Moo, L.R., Segal, J.B., Hart Jr., J., 2003. Distinct prefrontal cortex activity associated with item memory and source memory for visual shapes. Cogn. Brain Res. 17, 75–82.

Snyder, J.S., Yerkes, B., Pitts, M.A., 2015. Testing domain-general theories of perceptual awareness with auditory brain responses. Trends Cogn. Sci. 19, 295–297.

Stam, C.J., 2005. Nonlinear dynamical analysis of EEG and MEG: review of an emerging field. Clin. Neurophysiol. 116, 2266–2301.

Stefanics, G., Hangya, B., Hernádi, I., Winkler, I., Lakatos, P., Ulbert, I., 2010. Phase entrainment of human delta oscillations can mediate the effects of expectation on reaction speed. J. Neurosci. 30, 13578–13585.

Tallon-Baudry, C., Bertrand, O., Delpuech, C., Pernier, J., 1996. Stimulus specificity of phase-locked and non-phase-locked 40 Hz visual responses in human. J. Neurosci. 16, 4240–4249.

Taulu, S., Kajola, M., Simola, J., 2004. Suppression of interference and artifacts by the signal space separation method. Brain Topogr. 16, 269–275.

Tesche, C.D., Uusitalo, M.A., Ilmoniemi, R.J., Huotilainen, M., Kajola, M., Salonen, O., 1995. Signal-space projections of MEG data characterize both distributed and well localized neuronal sources. Electroencephalogr. Clin. Neurophysiol. 95, 189–200.

Thut, G., Schyns, P.G., Gross, J., 2011. Entrainment of perceptually relevant brain oscillations by non-invasive rhythmic stimulation of the human brain. Front. Psychol. 2, 170.

Thut, G., Miniussi, C., Gross, J., 2012. The functional importance of rhythmic activity in the brain. Curr. Biol. 22, R658–R663.

Uusitalo, M.A., Ilmoniemi, R.J., 1997. Signal-space projection method for separating MEG or EEG into components. Med. Biol. Eng. Comput. 35, 135–140.

van Dijk, H., Schoffelen, J.-M., Oostenveld, R., Jensen, O., 2008. Prestimulus oscillatory activity in the alpha band predicts visual discrimination ability. J. Neurosci. 28, 1816–1823.

van Ede, F., de Lange, F.P., Jensen, O., Maris, E., 2011. Orienting attention to an upcoming tactile event involves a spatially and temporally specific modulation of sensorimotor alpha- and beta-band oscillations. J. Neurosci. 31, 2016–2024.

Wallisch, P., Lusignan, M., Benayoun, M., Baker, T.I., Dickey, A.S., Hatsopoulos, N.G., 2009. Matlab for Neuroscientists. Elsevier Inc., California, USA.

Weisz, N., Obleser, J., 2014. Synchronisation signatures in the listening brain: a perspective from non-invasive neuroelectrophysiology. Hear. Res. 307, 16–28.

Weisz, N., Hartmann, T., Müller, N., Lorenz, I., Obleser, J., 2010. Alpha rhythms in audition: cognitive and clinical perspectives. Front. Psychol. 2, 73.

Womelsdorf, T., Valiante, T.A., Sahin, N.T., Miller, K.J., Tiesinga, P., 2014. Dynamic circuit motifs underlying rhythmic gain control, gating and integration. Nat. Neurosci. 17, 1031–1039.

Zhang, Y., Ding, M., 2010. Detection of a weak somatosensory stimulus: role of the prestimulus mu rhythm and its top-down modulation. J. Cogn. Neurosci. 22, 307–322.